

Universal quasi-Fermi liquid physics of one-dimensional interacting fermions

Joshua D. Baktay,¹ Adrian E. Feiguin,¹ and Julián Rincón²

¹*Department of Physics, Northeastern University, Boston, Massachusetts 02115, USA*

²*Department of Physics, Universidad de los Andes, Bogotá D.C. 111711, Colombia*

(Dated: June 17, 2024)

We present a class of one-dimensional generic spinless fermion lattice Hamiltonians that express quasi-Fermi liquid physics, manifesting both Luttinger and Fermi liquid features due to solely irrelevant interactions. Using infinite matrix product state techniques, we unveil its universal structure by calculating static and dynamic responses. Key features include a finite discontinuity in the momentum distribution at the Fermi level, despite power-law singularities in the spectral function protected by particle-hole symmetry. Away from half-filling Landau quasiparticles emerge. Charge dynamics show either high-energy bound states or concentration of spectral weight within the continuum for attractive or repulsive interactions, respectively. These universal features are realized across multiple models and energy scales thus reifying the quasi-Fermi liquid as a unique paradigm for one-dimensional fermions.

Introduction— Exploring exotic quantum phases is a central aim of condensed matter physics. One prime example is the Luttinger liquid (LL) [1], the paradigm for describing low-energy interacting electrons in one spatial dimension (1D). Contrary to Fermi liquids (FL), the prevailing theory to describe the problem in higher dimensions, the LL reveals an absence of Landau quasiparticles, instead manifesting only power-law singularities in the single-particle spectrum. Such a characteristic is universal: this defining phenomena is realized within a wide range of systems, regardless of microscopic details. Recently, a new regime of 1D physics has been demonstrated, known as quasi-Fermi liquids (qFL), manifesting signatures of both, LL and FL physics [2–4].

Physics beyond the LL paradigm has focused on reintroducing curvature of the dispersion relation to the linearized Luttinger model (known as nonlinear LL–nLL) [5–9]. In contrast, the qFL contains *only* irrelevant interactions in the renormalization group sense, in addition to the non-linear dispersion [2, 3]. Therefore, since fundamental properties are generally defined by the asymptotic behavior of propagators, a nLL and qFL occupy different universality classes: the former is perturbatively connected to the LL while the latter is perturbatively connected to a non-interacting system.

In this work, we present a class of microscopic spinless fermion lattice Hamiltonians that express qFL characteristics across various local interactions. We numerically study the ground state directly in the thermodynamic limit using uniform matrix product states (uMPS) and the variational uMPS (VUMPS) algorithm [10, 11]. We study the qFL excitations, namely the spectral function and dynamic structure factor (DSF), using tangent-space MPS methods [11–13]. Our results are further refined using finite-entanglement scaling (FES) [14–19]. By these means, we characterize the qFL in a generic class of models, reifying its robustness as a paradigm of 1D physics.

Models and Methods— We construct a class of interacting spinless fermion models on a 1D infinite lat-

tice, with general interactions over three contiguous lattice sites, and study their critical regime. The Hamiltonian characterizing this class is $H = \sum_{x \in \mathbb{Z}} H_x$, with local terms $H_x = -t(c_x^\dagger c_{x+1} + \text{H.c.}) + \mu n_x + H_x^{\text{int}}$. The hopping t and chemical potential μ define the couplings of the non-interacting part of H , setting the bandwidth and particle density, respectively. The interacting part $H_x^{\text{int}} = H_x^{i_1} + H_x^{i_2}$ is composed of two terms out of

$$H_x^{i_k} \in \left\{ V n_x n_{x+1}, t_c n_x (c_{x+1}^\dagger c_{x+2} + \text{H.c.}), \right. \\ \left. V_2 n_x n_{x+2}, t'_c (c_x^\dagger n_{x+1} c_{x+2} + \text{H.c.}) \right\}. \quad (1)$$

Parameters V and V_2 denote nearest and next-nearest neighbor interactions, respectively, with $n_x = c_x^\dagger c_x - 1/2$; t_c (t'_c) denote correlated hopping terms. All energies are expressed in units of t . We note that these are all the possible charge-conserving interactions in a spinless next-nearest neighbor model. We studied four combinations of H^{i_1} and H^{i_2} which we shall refer to by their couplings: Vt_c , V_2t_c , Vt'_c away from half filling [20], and VV_2 at half-filling. The VV_2 model away from half filling was explored in Ref. [4].

To study the ground state and excitations of H we utilized uMPS and tangent-space methods, which are translationally invariant and work directly in the thermodynamic limit [11, 21–23]. The representation power of these variational ansatzes (how close they can get to an arbitrary many-body state) is determined by their bond dimension, χ , that controls the number of variational parameters and defines a manifold as a subspace of the (exponentially-large) many-body Hilbert space. The VUMPS algorithm variationally finds the ground state within such manifold [10, 11]. The accuracy of the optimized uMPS is characterized by the energy density error, the discarded weight, and the norm of the tangent vector, which our simulations achieve around 10^{-12} , 10^{-10} , and 10^{-13} , respectively. In this work we use the so-called quasiparticle ansatz to study excitations [11–13]. We carried out simulations with bond dimensions up to $\chi = 640$

for the ground state and $\chi = 192$ for the excited states, keeping the entire excitation spectrum allowed by χ .

Finite χ imposes truncation effects on all calculations. We address this using FES [14–19], which allows us to further refine our results. By studying the behavior of expectation values as a function of χ , we can extrapolate our results to $\chi \rightarrow \infty$ which corresponds to the exact result. This FES analysis was done for all relevant calculations whose details are expounded upon below.

Results— For a generic system of interacting fermions, the qFL can be realized by setting the couplings of a lattice model such that marginal terms of the effective field theory are nullified, leaving the irrelevant terms to stabilize the state. Here, this is accomplished by exploring the interplay between H^{i_1} and H^{i_2} . This effective field theory is equivalent to that studied in Ref. [3], which omits marginal interactions a priori.

To this end, we first analyze the ground state of the class of models defined by H , following the recipe outlined in Ref. [4]. By judiciously searching the Hamiltonian parameter space of all models, we found continuous regions where the Luttinger parameter $K \simeq 1$ [24]. Of these families of parameter values, we find that all models exhibit a finite discontinuity in the momentum distribution at the Fermi momentum, k_F , which is a hallmark of FL. This is demonstrated by performing a FES study on the size of the discontinuity at k_F as $\chi \rightarrow \infty$. This stands in contrast to LL which manifest a power-law singularity. In what follows, we have selected representative sets of parameter values to study their excitations: $(V, V_2) = (-1.2, 1.2)$, $(V, t_c) = (-1.9, 0.8)$, $(V, t'_c) = (1.4, 0.8)$, $(V_2, t_c) = (-1, 0.8)$.

The presence of a discontinuity in the momentum distribution function for $K \simeq 1$ shows that the qFL ground state is perturbatively connected to free fermions. This is sensible given the asymptotics of the low-energy field theory: the marginal terms have been nullified and the irrelevant interactions vanish by definition for $k = k_F$.

Spectral Function— Single-particle excitations can be studied via the spectral function $A(k, \omega) = A_p(k, \omega) + A_h(k, \omega)$:

$$A_{p/h}(k, \omega) = \sum_{\alpha} |\langle \alpha | c_k^{(\dagger)} | 0 \rangle|^2 \delta(\omega \mp (E_{\alpha} - E_0)), \quad (2)$$

which include the particle (p) and hole (h) contributions, respectively. $|0\rangle$ is the ground state with energy E_0 , $|\alpha\rangle$ are excited states with one extra particle/hole with energy E_{α} , and $c_k^{(\dagger)}$ creates a particle/hole with momentum k . In a non-interacting system the spectral function consists of a delta peak that is broadened into a Lorentzian in the presence of interactions for dimensions $d > 1$, according to FL theory (in addition to an incoherent high energy background). In contrast, according to LL theory, in 1D interactions cause collective excitations resulting in power-law singularities [26–30].

Modifications beyond the linearized LL reintroduce the

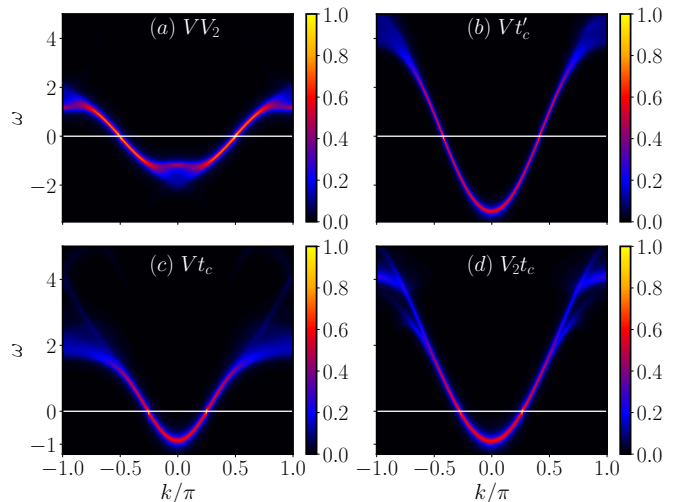


FIG. 1. Normalized spectral functions for four qFL models and their respective densities at $\chi = 104$ with the full excitation spectrum: (a) VV_2 , $n = 0.5$; (b) Vt'_c , $n = 0.41$; (c) Vt_c , $n = 0.25$; (d) V_2t_c , $n = 0.26$. The horizontal line indicates the Fermi level. Notice the particle-hole symmetry for the VV_2 model relative to the asymmetry of the others. At $k \sim 2k_F$ we see the formation of a high energy bound state [25].

previously omitted curvature, which is irrelevant in the renormalization group sense, alongside marginal interactions [7–9, 25, 31, 32]. Since the qFL contains only irrelevant interactions alongside the nonlinear dispersion, its excitations retain their quasiparticle nature as $k \rightarrow k_F$ instead of returning to the LL power-law [9].

At finite momentum, behavior in the particle and hole sectors varies depending on the quasiparticle group velocity, v , relative to the Fermi velocity, v_F [3]. For $v > v_F$, scattering is dispersive giving the excitation a finite lifetime and capping the spectral weight near the single-particle dispersion yielding a Lorentzian-like lineshape. This is possible because the irrelevant curvature allows the dispersion to now lie within the continuum of support [9]. For $v < v_F$, scattering is not dispersive and causes a proliferation of low-energy particle-hole pairs. Such behavior leads to an orthogonality catastrophe characteristic of LL and manifests as edge singularities accompanied by power-laws in the spectral function [3, 8, 30]. Thus, we summarize the hallmarks of a qFL as the presence of power-law singularities in *at least* one sector of the spectral function (despite the finite discontinuity in the momentum distribution) with the potential for quasiparticles in the opposite sector.

To show this for our class of generic Hamiltonians, we computed the spectral function using the quasiparticle ansatz [11–13, 24]. This ultimately amounts to a momentum-dependent eigenvalue problem whose energy spectrum scales with χ . The spectrum becomes continuous as $\chi \rightarrow \infty$ allowing for a faithful study of continuous dispersion. At finite χ the energy spectrum is discrete

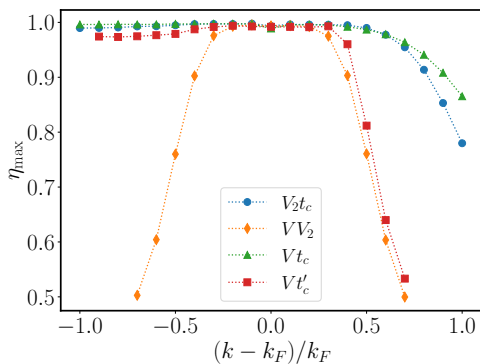


FIG. 2. FES extrapolated exponents as a function of momentum from k_F for the qFL models and parameters shown in Fig. 1. $\eta_{\max} = 1$ ($\eta_{\max} < 1$) corresponds to quasiparticle (power-law) excitations.

which requires the delta function of Eq. (2) to be replaced by Lorentzians with artificial broadening γ . So long as γ is larger than the level spacing we can mitigate finite-entanglement (finite- χ) effects. In the scaling limits $\chi \rightarrow \infty$, $\gamma \rightarrow 0$, we recover Eq. (2) exactly [24, 33].

Our results for the spectral functions can be seen in Fig. 1. The horizontal white line depicts the Fermi energy with hole excitations for $\omega < 0$, $|k| < k_F$ and particle excitations for $\omega > 0$, $|k| > k_F$.

The qFL signature described above can be seen in Fig. 2 depicting scaling exponents, η , as a function of momentum for the qFL class. Inspired by Ref. [33, 34], we can extract the exponents from spectral momentum cuts by observing how the spectral weight at the peak maximum scales with ξ (the correlation length of the ground-state uMPS transfer matrix) and the artificial broadening γ . First performing the γ -scaling to extract η_{\max} for a series of fixed ξ we then extrapolate to $\xi \rightarrow \infty$ by fitting η_{\max} against $\xi^{-1}(\chi)$. The obtained exponents characterize the nature of the particle and hole sectors as a function of momentum: $0 < \eta_{\max} < 1$ indicates power-laws and $\eta_{\max} \simeq 1$ specifies quasiparticles.

In three of the four models we see the *mixed* qFL signature described above: quasiparticles in the hole sector and power-laws in the particle sector. Away from half filling, the asymmetry between the sectors is determined by the group velocity of the quasiparticles. For generic dispersions with density $n < 1/2$ one typically expects $v < v_F$ for a hole. Thus, one might always expect power-law edge singularities in the hole sector. However, approximating the dispersion to second order can yield, in the strongly-interacting regime, an effective mass with sign opposite to v_F [5, 25], flipping the sign of v relative to v_F . Note, additionally, one can swap the behavior of the sectors under a particle-hole transformation. In the VV_2 model we realize the *full* qFL signature as power-laws in both sectors due to protection of particle-hole symmetry at half-filling. In this case, the dispersion coincides with

the edge of the spectral support in both sectors [9].

For all models, the decrease in η_{\max} in the power-law sectors is due to the momentum-dependence of the couplings within the effective field theory [3]. As k increases the coupling increases along with the severity of the power-law. As $k \rightarrow k_F$ the coupling goes to zero, the irrelevant terms vanish, and $\eta_{\max} \rightarrow 1$. We confirm this asymptotic behavior by computing η_{\max} directly at $k = 0$ which demonstrates the universality of the qFL.

Dynamic Structure Factor— We compute the DSF as the momentum-frequency-resolved density-density correlation function,

$$S(q, \omega) = \sum_{\alpha} |\langle \alpha | \rho_q | 0 \rangle|^2 \delta(\omega - (E_{\alpha} - E_0)), \quad (3)$$

where ρ_q creates a particle-hole excitation of momentum q on top of the ground state. Again, at finite χ the delta must be replaced by a Lorentzian with broadening γ . This allows for smooth momentum cuts with oscillations that reflect the artificially discrete spectrum due to finite χ . The DSF for the qFL class can be seen in Fig. 3, from which universal features can be extracted at length scales differentiated by $q \sim \pi - 2k_F$ as an approximate switch between the two and three branch regimes (for densities < 0.5). The branches correspond to thresholds that define the support of the two-particle spectrum [25].

For $q \lesssim \pi - 2k_F$ we observe the expected quadratic broadening of the linear sound mode for all models due to the nonlinear dispersion and irrelevant interactions [5, 35]. This demonstrates the free-fermion-like nature of the qFL at low energies. In addition, DSF spectral weight is concentrated on the upper threshold of the spectrum, similar to free fermions [24].

For $q \gtrsim \pi - 2k_F$, nullification of marginal terms at low energies breaks down and the larger Hamiltonian parameter in absolute value, within H^{i1} and H^{i2} , dominates whose positive (negative) sign causes a net repulsive (attractive) behavior. This is most apparent through the behavior of the branches. For the net attractive models with the negative parameter of H^{i1} (VV_2 [36], Vt_c , V_2t_c , Fig. 3a-d), the spectral weight is concentrated in the upper branch, reminiscent of the bound state/magnon dispersion of the attractive tV /ferromagnetic XXZ model [37–39]. For the net repulsive model with the positive parameter of H^{i1} (Vt'_c , Fig. 3b), the spectral weight is instead concentrated in the middle branch, reminiscent of the repulsive tV model [25, 40, 41].

To make this notion more rigorous, we plot the free-fermion and magnon dispersions on top of the colormaps and note regions of similarity with the branches [25, 38]. Using a bandwidth J_{eff} for the free-fermion dispersion (computed from the Fermi velocity of the qFL spectral function), we note a general matching with the three branches of the Vt'_c model. Additionally, by kinematic constraints, the lower free-fermion branch remains the

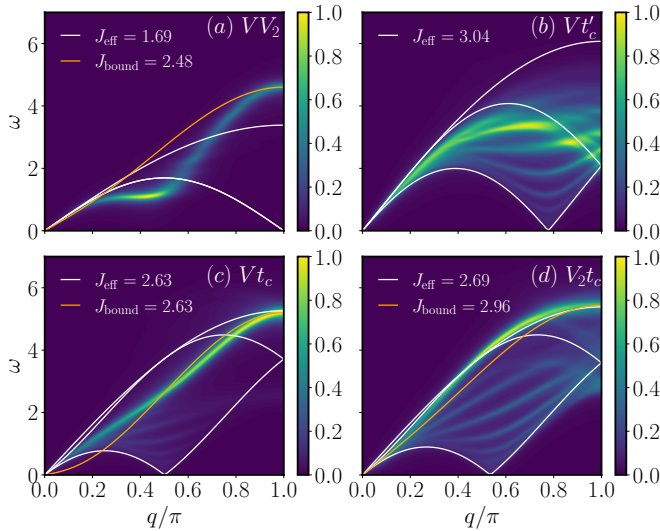


FIG. 3. Normalized dynamic structure factor for four qFL models at $\chi = 104$ with full excitation spectrum: (a) VV_2 , (b) Vt'_c [42], (c) Vt_c , (d) V_2t_c . There are two branches at half-filling (a) and three otherwise (b)-(d). Note the dominant upper branch in (a), (c), and (d) above a faint continuum (see also Fig. 4a,b), which mimics the *attractive* tV model, suggesting bound states. Next, note the dominant middle branch in (b) along with faint upper and lower branches, mimicking the *repulsive* tV model. Strengthening the comparison, we plot the free-fermion dispersion (white) using the renormalized bandwidth J_{eff} calculated from $A(k, \omega)$, as well as the ferromagnetic XXZ magnon dispersion (orange); J_{bound} is fit to the energy scale. At finite χ , each continuum is distributed over discrete lines that fuse into a smooth region as $\chi \rightarrow \infty$.

lower boundary of spectral support for all models away from half-filling. Finally, using J_{bound} to fit the magnon dispersion, we note a qualitative agreement with the curvature of the upper branches for the net attractive models, again suggestive of bound-state/excitonic physics due to an effective negative interaction parameter [37–39].

To further probe the physics in this high-energy regime, we study the lineshape of several momentum cuts. In addition to S_{max} , we also examine how the half-width-half-maximum, $\sigma_{\pm} = |\omega_{\pm} - \omega_{\text{max}}|$, scales with γ , where $\omega_{\text{max}, \pm}$ are defined as $S_q(\omega_{\text{max}}) = S_{\text{max}}$ and $S_q(\omega_{\pm}) = S_{\text{max}}/2$. Here, we perform the γ and χ scaling limits concurrently through the ansatz $\gamma(\xi) = c/\xi(\chi)$, which adapts finite-size methods to uMPS. $c > 0$ is chosen to balance the spectrum resolution ($\sim \xi^{-1}$) with the physically relevant features of the lineshape [24, 33]. Similar to the spectral function, we extract scaling exponents η_{max} as the slope of $\ln S_{\text{max}}(\ln \gamma)$. From $\sigma_{\pm}(\gamma)$, slopes $\Sigma_{\pm} \sim 1$ again characterize Lorentzians while $\Sigma_{\pm} \neq 1$ denote power-laws. Together these quantities capture the qualitative changes in the lineshape with q .

In Fig. 4 we show $\eta_{\text{max}}(q)$, $\Sigma_{\pm}(q)$ for the attractive-qFL with dominant upper branches: VV_2 , Vt_c , V_2t_c . As remarked above, we hypothesize exciton-like physics in

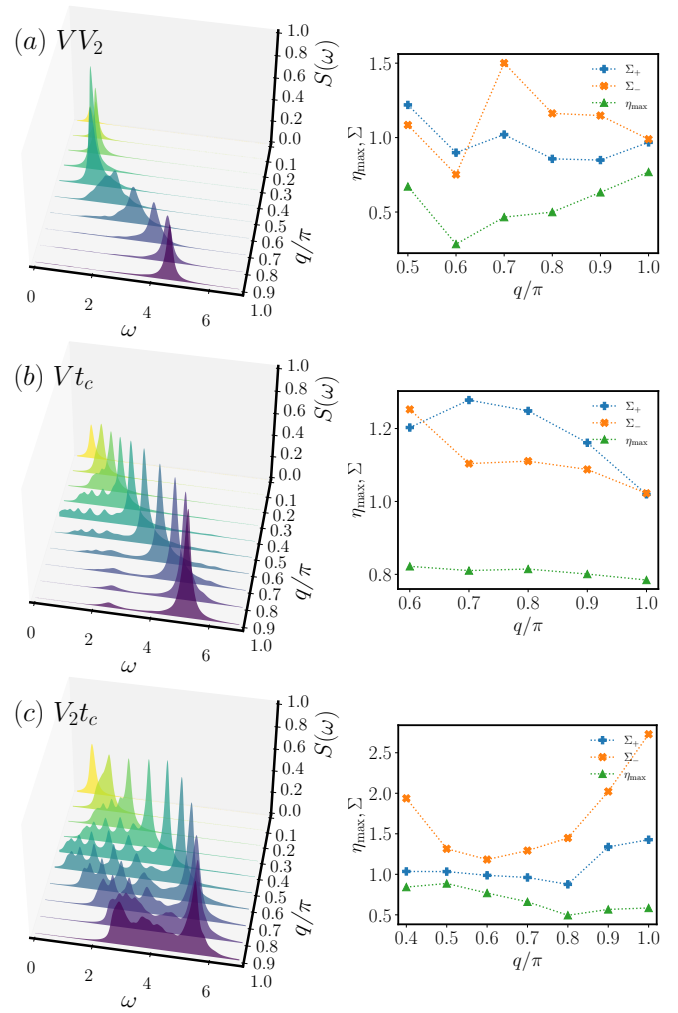


FIG. 4. FES extrapolated exponents, η_{max} , and half-width-maximum scaling, Σ_{\pm} , as a function of momentum (right column) of the peaks in the corresponding momentum cuts (left column) for the three attractive qFL models. The value of c in the scaling law $\gamma = c/\xi(\chi)$ is model dependent: (a) VV_2 , $c = 15$; (b) Vt_c , $c = 45$; (c) V_2t_c , $c = 20$. For (a)-(b), as $q \rightarrow \pi$ the lineshape evolve toward a symmetric, Lorentzian-like peak. In (c) we have a similar behavior instead near $q = 0.6\pi$. This is reflected in $\Sigma \rightarrow 1$. Given effective attractive interactions, this peak represents an exciton whose hybridization with the surrounding excitations causes $\eta_{\text{max}} < 1$.

this upper branch. This exciton originates from particle-hole symmetric two-particle excitations. To see this, observe that $\Sigma_{\pm} \rightarrow 1$ for specific momentum values in the high energy regime. This mirrors the lineshape evolution toward more symmetric, Lorentzian-like peaks, suggesting quasiparticle behavior for the particle-hole bound state represented by this upper branch. However, $\eta_{\text{max}} \not\sim 1$. Its difference from unity is due to its hybridization with the continuum. This hybridization decreases as the energy-separation between the peak and the continuum increases and/or the spectral weight of the continuum itself decreases. Indeed, the DSF of the attractive

tV model possesses a fully disconnected bound state in the same momentum regime [39] and yields $\eta_{\max} \sim 1$, $\Sigma_{\pm} \sim 1$ (not shown). All this suggests that this hybridized exciton is a universal feature of attractive-qFL models such that true quasiparticle behavior is not possible while maintaining the $K = 1$ constraint. In contrast, absence of the exciton is a universal feature of repulsive-qFL models [24] in line with physics of the repulsive tV model [38, 40, 41, 43].

Conclusion— We have computed static and dynamic correlations for a class of lattice Hamiltonians realizing the universal features of the qFL. These most significantly consist of a finite discontinuity in the momentum distribution, despite the presence of power-law singularities in the spectral function. Away from half-filling, these models also display Landau quasiparticles. These disparate features shared across this class solidify the qFL as a robust phase of correlated 1D systems beyond the LL paradigm. In addition, the dynamic structure factor reveals bound states near the upper threshold for attractive systems, while repulsive ones localize spectral weight within the two-particle continuum. Finally, preliminary results (not shown) indicate that including additional Hamiltonian terms (such as next-nearest neighbor hopping) can also yield $K \sim 1$ regions in parameter space.

JDB, AEF, and JR thank A. Rozhkov for previous collaboration and fruitful discussions. AEF and JDB acknowledge support from the U.S. Department of Energy, Office of Basic Energy Sciences under grant No. DE-SC0014407 (AEF and JDB). JR acknowledges support from the Office of the Vice-president of Research and Creative Activities and the Office of the Faculty of Science Vice-president of Research of Universidad de los Andes under the FAPA grant. Computational cluster research conducted as part of a user project at the Center for Nanophase Materials Sciences (CNMS), which is a US Department of Energy, Office of Science User Facility at Oak Ridge National Laboratory.

-
- [1] F. D. M. Haldane, *J. Phys. C: Solid State Phys.* **14**, 2585 (1981).
- [2] A. V. Rozhkov, *Phys. Rev. B* **74**, 245123 (2006).
- [3] A. V. Rozhkov, *Phys. Rev. Lett.* **112**, 106403 (2014), see also [Supplemental Material](#).
- [4] J. D. Baktay, A. V. Rozhkov, A. E. Feiguin, and J. Rincón, *Phys. Rev. B* **108**, 245134 (2023).
- [5] R. G. Pereira, J. Sirker, J.-S. Caux, R. Hagemans, J. M. Maillet, S. R. White, and I. Affleck, *J. Stat. Mech.* **2007**, P08022 (2007).
- [6] R. G. Pereira, *Int. J. Mod. Phys. B* **26**, 1244008 (2012).
- [7] A. Imambekov, T. L. Schmidt, and L. I. Glazman, *Rev. Mod. Phys.* **84**, 1253 (2012).
- [8] M. Pustilnik, M. Khodas, A. Kamenev, and L. I. Glazman, *Phys. Rev. Lett.* **96**, 196405 (2006).
- [9] M. Khodas, M. Pustilnik, A. Kamenev, and L. I. Glazman, *Phys. Rev. B* **76**, 155402 (2007).
- [10] V. Zauner-Stauber, L. Vanderstraeten, M. T. Fishman, F. Verstraete, and J. Haegeman, *Phys. Rev. B* **97**, 045145 (2018).
- [11] L. Vanderstraeten, J. Haegeman, and F. Verstraete, *SciPost Phys. Lect. Notes*, **7** (2019).
- [12] J. Haegeman, B. Pirvu, D. J. Weir, J. I. Cirac, T. J. Osborne, H. Verschelde, and F. Verstraete, *Phys. Rev. B* **85**, 100408 (2012).
- [13] J. Haegeman, T. J. Osborne, and F. Verstraete, *Phys. Rev. B* **88**, 075133 (2013).
- [14] L. Tagliacozzo, T. R. de Oliveira, S. Iblisdir, and J. I. Latorre, *Phys. Rev. B* **78**, 024410 (2008).
- [15] F. Pollmann, S. Mukerjee, A. M. Turner, and J. E. Moore, *Phys. Rev. Lett.* **102**, 255701 (2009).
- [16] B. Pirvu, G. Vidal, F. Verstraete, and L. Tagliacozzo, *Phys. Rev. B* **86**, 075117 (2012).
- [17] V. Stojevic, J. Haegeman, I. P. McCulloch, L. Tagliacozzo, and F. Verstraete, *Phys. Rev. B* **91**, 035120 (2015).
- [18] M. M. Rams, P. Czarnik, and L. Cincio, *Phys. Rev. X* **8**, 041033 (2018).
- [19] B. Vanhecke, J. Haegeman, K. Van Acoleyen, L. Vanderstraeten, and F. Verstraete, *Phys. Rev. Lett.* **123**, 250604 (2019).
- [20] The Vt'_c model is equivalent to the J_1 - J_2 Heisenberg model under Jordan-Wigner transformation.
- [21] G. Vidal, *Phys. Rev. Lett.* **98**, 070201 (2007).
- [22] J. Haegeman, J. I. Cirac, T. J. Osborne, I. Pizorn, H. Verschelde, and F. Verstraete, *Phys. Rev. Lett.* **107**, 070601 (2011).
- [23] J. I. Cirac, D. Pérez-García, N. Schuch, and F. Verstraete, *Rev. Mod. Phys.* **93**, 045003 (2021).
- [24] See Supplemental Materials at [URL will be inserted by publisher] for phase diagrams of the Luttinger parameter, static correlation functions, numerical details of the excitations, and supporting analysis of the DSF.
- [25] R. G. Pereira, S. R. White, and I. Affleck, *Phys. Rev. B* **79**, 165113 (2009).
- [26] I. E. Dzyaloshinskii and A. I. Larkin, *Sov. Phys. JETP* **38**, 202 (1974).
- [27] A. Luther and I. Peschel, *Phys. Rev. B* **9**, 2911 (1974).
- [28] V. Meden and K. Schönhammer, *Phys. Rev. B* **46**, 15753 (1992).
- [29] J. Voit, *Phys. Rev. B* **47**, 6740 (1993).
- [30] T. Giamarchi, *Quantum Physics in One Dimension* (Oxford University Press, 2003).
- [31] A. Imambekov and L. I. Glazman, *Phys. Rev. Lett.* **102**, 126405 (2009).
- [32] A. Imambekov and L. I. Glazman, *Science* **323**, 228 (2009).
- [33] E. Jeckelmann, *Phys. Rev. B* **66**, 045114 (2002).
- [34] H. Benthien, F. Gebhard, and E. Jeckelmann, *Phys. Rev. Lett.* **92**, 256401 (2004).
- [35] A. V. Rozhkov, *Eur. Phys. J. B* **47**, 193 (2005).
- [36] For the VV_2 model the parameters chosen are equal in value. We understand this by considering V_2 , which acts over two sites, to be half as strong relative to V analogous to a Coulomb interaction.
- [37] V. S. Viswanath, S. Zhang, G. Müller, and J. Stolze, *Phys. Rev. B* **51**, 368 (1995).
- [38] F. Franchini, *An Introduction to Integrable Techniques for One-Dimensional Quantum Systems* (Springer Cham, 2017).

- [39] R. G. Pereira, S. R. White, and I. Affleck, *Phys. Rev. Lett.* **100**, 027206 (2008).
- [40] J.-S. Caux and J. M. Maillet, *Phys. Rev. Lett.* **95**, 077201 (2005).
- [41] J.-S. Caux, R. Hagemans, and J. M. Maillet, *J. Stat. Mech.* **2005**, P09003 (2005).
- [42] The DSF for Vt'_c used parameter values that are half of those listed in the main text; they still reside in the qFL region and the DSF features are qualitatively the same while being slightly more discernable.
- [43] J.-S. Caux, H. Konno, M. Sorrell, and R. Weston, *Phys. Rev. Lett.* **106**, 217203 (2011).

Supplemental Material for “Universal quasi-Fermi liquid physics of one-dimensional interacting fermions”

Joshua D. Baktay,¹ Adrian E. Feiguin,¹ and Julián Rincón²

¹*Department of Physics, Northeastern University, Boston, Massachusetts 02115, USA*

²*Department of Physics, Universidad de los Andes, Bogotá D.C. 111711, Colombia*

(Dated: June 17, 2024)

S1. INTRODUCTION

In the main text we characterized the excited states of quasi-Fermi liquid (qFL) systems. There we observed its universal signatures in the spectral function, as critical excitations in at least one sector whose exponents decrease with increasing momentum. We also showed that the dynamic structure factor (DSF) displays an upper branch for systems with an attractive effective interaction, associated with particle-hole excitations that are particle-hole symmetric. Here we present a complete characterization of the qFL ground state, according to Ref. [1]. This demonstrates the other universal features of the qFL. Finally, we provide some supporting analysis for the DSF.

S2. GROUND STATE ANALYSIS

In accordance with the vanishment of irrelevant interactions in the infrared limit, the qFL ground state is perturbatively connected to the ground state of the free Fermi gas. Therefore, we might expect its Luttinger parameter $K = 1$, which accounts for the nature and strength of the interactions. It follows from Luttinger liquid (LL) theory that K can be extracted as a low-momentum, linear approximation of the charge structure factor (CSF): the Fourier transform of the density-density correlation function,

$$D(k) = \sum_j \langle n_0 n_j \rangle e^{-ikj}. \quad (\text{S1})$$

Using the uniform matrix product state (uMPS) approximation to the ground state to compute the expectation value $\langle n_0 n_j \rangle$, and therefore $D(k)$, K can be extracted from its slope near $k \rightarrow 0^+$ as $dD(k)/dk = K/2\pi$ [2]. Thus, a judicious grid search was performed in Hamiltonian parameter space where K was extracted from the CSF for each set of parameter values for each model of the qFL class. The results are shown in Fig. S1. For each model we observe a continuous region of parameters where $K \simeq 1$. This represents a family of qFL candidates where the parameter values are tuned relative to each other to stabilize the state.

The contour of each region reveals an important point about the generality of the qFL physics. In none of our four models are the qFL parameters commensurate in

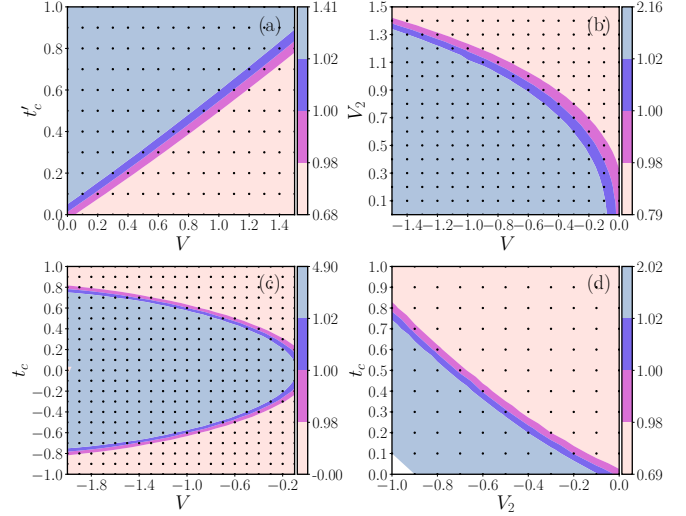


FIG. S1. Phase diagram of the Luttinger parameter, K , for all four qFL models at (a) $\mu/t = 1.0$, (b) $\mu/t = 0$, (c) $\mu/t = 0$, (d) $\mu/t = 1.0$. The qFL is stable along each band where $0.98 \leq K \leq 1.02$. The relaxation of the strict $K = 1$ constraint demonstrates the robustness of the qFL phase. For $K < 1$ ($K > 1$) the ground state is dominated by charge-ordered (superconducting) fluctuations. In (c) we demonstrate the preservation of the qFL band under particle-hole exchange through its reflection about the $t_c = 0$ axis (which also occurs for the Vt_c model—not shown). From these bands we chose the following representative values for further study: $(V, t_c) = (1.4, 0.8)$, $(V, V_2) = (-1.2, 1.2)$, $(V, t_c) = (-1.9, 0.8)$, $(V_2, t_c) = (-1, 0.8)$.

value which one might expect given that such parameter tuning serves to nullify marginal interactions. This illustrates that the qFL behavior is independent of a particular microscopic mechanism (like the intuitive competition between attractive and repulsive interactions) and instead depends purely on the effective couplings in the infrared limit.

The CSF of four representative candidates for each model is presented in Fig. S2a. The smooth behavior indicates a metallic state, and the deviations at high momenta from the plateau-like trend of free fermions signify interactions. In the insets we show the finite-entanglement scaling of K as a function of the uMPS correlation length ξ . This allows us to extrapolate our approximate value of K to the infinite- χ limit corresponding to the exact value. With the high statistical correlation of the linear fit we are confident in our results.

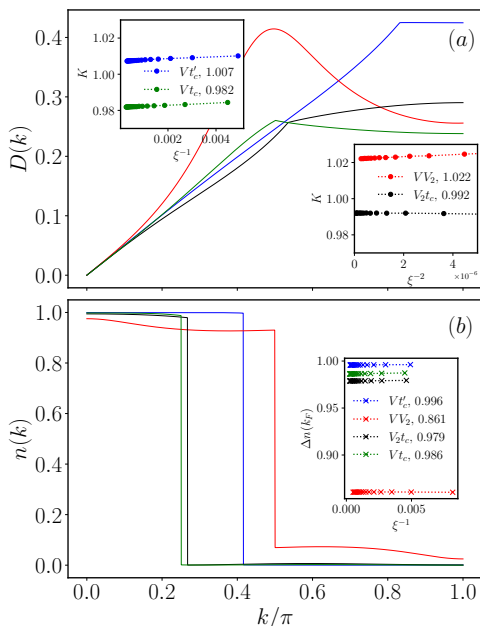


FIG. S2. (a) Static structure factor $D(k)$ and (b) momentum distribution $n(k)$ for the representatives of all four qFL models. The insets show the FES analysis for the Luttinger parameter K and the size of the discontinuity, $\Delta n(k_F)$. $K = 1.00(2)$ along with a finite $\Delta n(k_F)$ for $\chi \rightarrow \infty$ confirms the qFL region in Fig. S1. The different scaling exponents for ξ define their relationship to χ and is in general model dependent.

Remarkably, note that K for the Vt_c and VV_2 models is not strictly 1, differing by $\approx 2\%$. This implies that strict calibration of Hamiltonian parameters is not necessary to realize the qFL, and may make an experimental realization more tractable.

Next, we calculated the momentum distribution function, $n(k)$,

$$n(k) = \sum_j \langle c_0^\dagger c_j \rangle e^{-ikj}, \quad (\text{S2})$$

similarly to the CSF [3], which can be seen in Fig. S2b. As was shown in Ref. [4], the qFL ground state (again being perturbatively connected to free fermions) possesses a finite discontinuity in $n(k)$ at the Fermi point, k_F , in stark contrast to the kink power-law singularity of a LL. In order to show this we examined the finite-entanglement scaling (FES) of the size of the discontinuity about k_F . Specifically, we computed it as

$$\Delta n(k_F) := n(k_F - \pi/\xi(\chi)) - n(k_F + \pi/\xi(\chi)) \quad (\text{S3})$$

where $\xi(\chi)$ is the correlation length computed from the uMPS transfer matrix as a function of the bond dimension, χ . Given the inherently limited resolution of a finite- χ data set, a FES analysis was performed on $\Delta n(k_F)$ for each model. This can be seen in the inset of Fig. S2b, where $\Delta n(k_F)$ clearly extrapolates to finite values as $\xi(\chi) \rightarrow \infty$.

The finite discontinuity in $n(k_F)$ along with $K = 1$ as $\xi(\chi) \rightarrow \infty$ completes the qFL ground state characterization of our class of Hamiltonian models.

S3. ENTANGLEMENT SCALING FOR DYNAMIC CORRELATION FUNCTIONS

Let us discuss the extension of finite-entanglement scaling analysis to the realm of dynamic correlations computed using MPS, which we exploited to characterize the excitations of the qFL. The core idea of finite-entanglement scaling is based on the fact that the MPS correlation length, $\xi = \xi(\chi)$ diverges as $\chi \rightarrow \infty$, and that all observables obey scaling laws as a function of ξ [5, 6]. This idea can also be posed in terms of the vanishment of the level spacing of the eigenvalues of the MPS transfer matrix as $\chi \rightarrow \infty$. This is fundamental when studying critical systems where no finite-length scales exist.

For concreteness, suppose we want to accurately compute the dynamic correlation function of operator O_q with momentum q at energy ω ,

$$D_O(q, \omega) = \sum_\alpha |\langle 0|O_q|\alpha \rangle|^2 \delta(\omega - \omega_\alpha(q)), \quad (\text{S4})$$

where we have used the Lehmann representation. Here, $|0\rangle$ and $|\alpha\rangle$ stand for the ground state and excitations of energy $\omega_\alpha(q)$ with respect to the ground state energy. The so-called spectral weight or form factor is defined by the overlap $W(s, q) = |\langle 0|O_q|\alpha \rangle|^2$. We can compute this quantity using MPS methods, such as the quasiparticle ansatz, which approximate excited states with finite entanglement and, hence, finite resolution $\gamma > 0$. The form of the dynamic correlation under such an approximation and exploiting translation invariance is

$$D_O^{\xi, \gamma}(q, \omega) \approx \sum_\alpha W_\xi(\alpha, q) \frac{\gamma}{[\omega - \omega_{\alpha, \xi}(q)]^2 + \gamma^2}, \quad (\text{S5})$$

where the excitation energy $\omega_{\alpha, \xi}(q)$ and the form factor $W_\xi(\alpha, q) = |\langle \Psi(A)|O_0|\Phi_q^\alpha(B)\rangle|^2$ depend on ξ , again, because of the finiteness of χ . The operator O_0 is now located at an arbitrary site 0. The ground and excited states have been approximated with a uMPS

$$|\Psi(A)\rangle = \sum_{\{s\}} \left(\prod_{m \in \mathbb{Z}} A^{s_m} \right) |\{s\}\rangle,$$

and a quasiparticle ansatz state [3, 7]

$$|\Phi_q(B)\rangle = \sum_{n, \{s\}} e^{iqn} \left[\prod_{m < n} A_L^{s_m} \right] B^{s_n} \left[\prod_{m > n} A_R^{s_m} \right] |\{s\}\rangle,$$

where A and B are rank-three tensors, of dimension $\chi^2 d$, containing the variational parameters of the ground and excited states, respectively. B represents a local perturbation on top of the uMPS ground state. In accordance

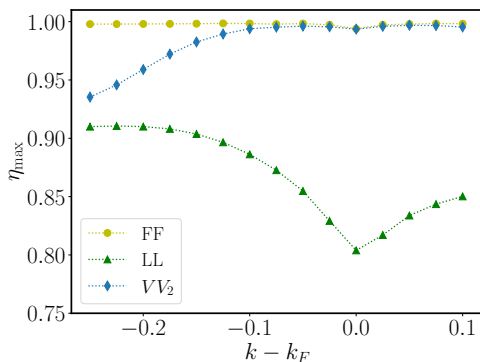


FIG. S3. Extrapolated scaling exponents as a function of momentum for the models presented in Ref. [1]. The FES analysis was performed as in the main text for bond dimensions up to $\chi = 160$. The VV_2 qFL has a density of $n = 0.3$ which breaks particle-hole symmetry and manifests the *mixed* qFL signature: power-laws in only one sector, quasiparticles in the other. Contrary to the models in the main text, we find the collective excitations in the hole sector (see main text).

with uMPS, we operate in the thermodynamic limit and thus the excitations have a well-defined momentum, q .

The finite-entanglement scaling technique for dynamic correlation functions then consists of generating sequences of data for $D_O^{\xi, \gamma}$ for pairs (ξ, γ) , and studying its scaling behavior (how it changes as a function of ξ and γ). It is expected that in the scaling limits $\xi \rightarrow \infty$ and $\gamma \rightarrow 0$ a construction of D_O will be possible. Most generally the limit of ξ must precede that of γ . Indeed, if D_O possesses a continuous spectrum, then for finite ξ , equivalently finite χ , if $\gamma \rightarrow 0$ the spectrum will be discrete and the lineshape will not be smooth. On the contrary, if the spectrum is discrete then we can safely evaluate the limit $\gamma \rightarrow 0$ first.

We require for the broadening γ to always be larger than the largest level spacing, $\Delta\omega_{\alpha, \xi}$, of the excitation spectrum, i.e. $\gamma > \Delta\omega_{\alpha, \xi}$ for fixed $\xi(\chi)$. Notice that as $\xi \rightarrow \infty$, $\Delta\omega_{\alpha, \xi} \rightarrow 0$, so the spectral response is smoothed out and closely resembles the exact result. Further requirements for γ can be imposed depending on the scaling procedure utilized (see below).

The finite-entanglement scaling behavior of our MPS-represented dynamic correlations is first demonstrated by computing the γ and ξ limits not concurrently as follows [always maintaining $\gamma > \Delta\omega_{\alpha, \xi}$]. It can be shown that the maximum, which occurs at $\omega = \omega_\alpha(q)$, of the convolution of D_O with a Lorentzian diverges as $\gamma^{-\eta}$. The exponent satisfies $\eta = 1$ ($\eta < 1$) for quasiparticle (power-law) excitations. Thus, for fixed $\xi(\chi)$, one can extract an approximate η for a decreasing sequence of γ values (an analogous technique was done in Ref. [1] albeit for fixed system size). Subsequently, the entanglement scaling occurs by generating a sequence of values for ξ and extrapolating η as a function of ξ .

A more efficient and potentially more accurate approach is perform the γ and ξ limits concurrently by

using a broadening that depends on χ : $\gamma = \gamma(\chi) > 0$, and goes to zero as $\xi \rightarrow \infty$. Leveraging previous work on finite-size scaling of dynamic correlation functions [8], we propose the broadening function

$$\gamma(\xi) := \frac{c}{\xi^\eta}, \quad (\text{S6})$$

where $c > 0$ is a χ -independent parameter freely chosen to ensure $\gamma(\xi) > \Delta\omega_{\alpha, \xi}$. Note that $\xi \rightarrow \infty$, as $\chi \rightarrow \infty$, so $\gamma(\xi) \rightarrow 0$, yielding an estimation of η . In this alternative approach, generating a sequence of ξ values automatically guarantees a sequence for γ that ensures that the scaling limits are satisfied.

S4. EXCITATIONS ANALYSIS

SA. Spectral function results

In Fig. S3 we reproduce the results of Ref. [1] in order to benchmark the method described in the main text. The spectral function results of Ref. [1] were computed for a finite-size system using time-dependent density matrix renormalization group (tDMRG), where only the γ scaling was performed at fixed chain length. Thus our results improve on the previous in two ways: (1) they were calculated in the infinite-chain (thermodynamic) limit and (2) both the γ and χ scaling limits were performed. The agreement between the two methods both confirms the validity of our method while also demonstrating that the finite-chain results survive in the infinite length limit.

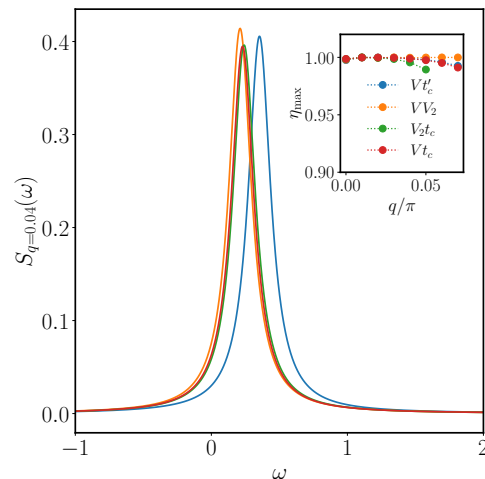


FIG. S4. Momentum cuts of the dynamic structure factor at $q = 0.04\pi \ll k_F$ for the qFL class of models presented in the main text at $\chi = 104$ and artificial broadening $\gamma = 0.1$. The Lorentzian lineshape confirmed by the scaling exponents in the inset confirms the presence of a sound mode for $q \ll k_F$.

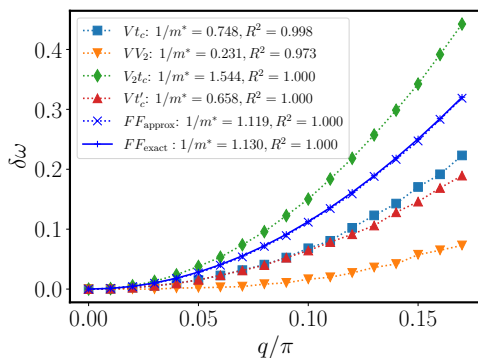


FIG. S5. Quadratic fits of the bandwidth, $\delta\omega(q)$, as a function of momentum for the qFL models compared to free fermions at $\chi = 104$. For free fermions, we computed $\delta\omega(q)$ using both the exact dispersion and our simulations. The agreement between the two indicates the accuracy of our methods. For $q < k_F$ the bandwidth is significantly narrower relative to the continuum at higher momenta. Therefore, the density of excitations is much higher allowing for much more accurate results at the same bond dimension.

SB. Dynamic structure factor results

In Fig. S4 we present momentum cuts of the sound mode (low momentum region) for each Hamiltonian model of the qFL class, with fixed selected parameters, discussed in the main text. The clearly delta lineshape (which manifests in our calculations as a Lorentzian due to convolution) is confirmed by the inset where we show that the FES extrapolated scaling exponents $\eta_{\max} \sim 1$ for $q \ll k_F$. These exponents were computed by employing only the scaling limit for the broadening γ at fixed χ , or equivalently and in practice fixed ξ , which is sufficient for the purposes of our analysis.

According to Refs. [9, 10], the presence of irrelevant operators like a nonlinear dispersion, or irrelevant interactions, introduces interactions between the LL bosons causing a quadratic broadening of the bandwidth in the DSF at low momentum that scales as:

$$\delta\omega(q) = \omega_U(q) - \omega_L(q) = \frac{1}{|m^*|} q^2, \quad (\text{S7})$$

where m^* is the effective mass, which can take positive and negative values, and $\omega_{L/U}(q)$ are the lower and upper boundaries of finite support in the DSF.

In Fig. S5 we show $\delta\omega(q)$ for our qFL class of Hamiltonian models. The high correlation coefficients demon-

strate that the DSF for our qFL all exhibit the same quadratic broadening, as expected from the general discussion above.

The broadening result for free fermions is $\delta\omega(q) \approx (J \cos k_F) q^2$. Exploiting this result we can use our estimates of the effective mass $1/|m^*|$ to predict the densities of our models and compare to the known densities: $n_{\text{predicted}} = \{0.393, 0.219, 0.378, 0.462\}$, $n_{\text{known}} = \{0.389, 0.268, 0.251, 0.500\}$ for the Vt'_c , V_2t_c , Vt_c , VV_2 models, respectively. From this we see a striking agreement for Vt'_c compared to the other three. This indicates that the low-energy behavior of the Vt'_c model is closer to a true free fermionic theory; the other three are more closely described by a free fermionic theory under the influence of irrelevant interactions, which we interpret as a Fermi liquid. This is reflected in the momentum distribution (see Fig. S2) where Vt'_c is much closer to true step function with $\Delta n(k_F) \sim 1$.

Finally, in Fig. S6 we show a series of lineshapes for the repulsive qFL, Vt'_c . Contrary to the attractive qFL models there is no high-energy bound state dispersion curve. Instead, the spectral weight accumulates in the middle of the continuum. The colormap in the main text suggests that this accumulation corresponds to a middle dispersion branch analogous to the repulsive tV model.

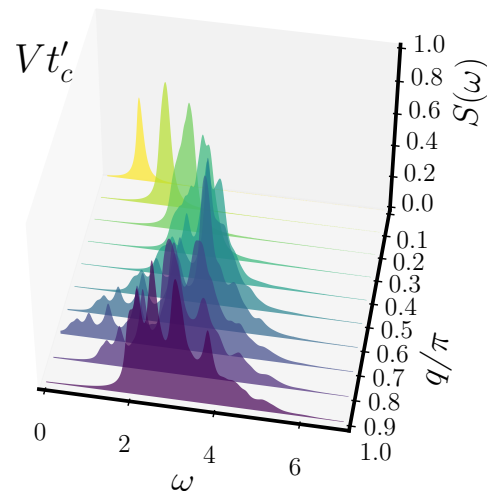


FIG. S6. DSF lineshapes for different momentum values for the repulsive Vt'_c qFL model. In contrast to the attractive qFL models discussed in the main text, as $q \rightarrow \pi$ the lineshapes accumulate spectral weight at intermediate energies.

[1] J. D. Baktay, A. V. Rozhkov, A. E. Feiguin, and J. Rincón, *Phys. Rev. B* **108**, 245134 (2023).
 [2] T. Giamarchi, *Quantum Physics in One Dimension* (Oxford University Press, 2003).
 [3] L. Vanderstraeten, J. Haegeman, and F. Verstraete, *SciPost Phys. Lect. Notes*, 7 (2019).

[4] A. V. Rozhkov, *Phys. Rev. Lett.* **112**, 106403 (2014), see also [Supplemental Material](#).
 [5] L. Tagliacozzo, T. R. de Oliveira, S. Iblisdir, and J. I. Latorre, *Phys. Rev. B* **78**, 024410 (2008).
 [6] F. Pollmann, S. Mukerjee, A. M. Turner, and J. E. Moore, *Phys. Rev. Lett.* **102**, 255701 (2009).

- [7] J. Haegeman, B. Pirvu, D. J. Weir, J. I. Cirac, T. J. Osborne, H. Verschelde, and F. Verstraete, *Phys. Rev. B* **85**, 100408 (2012).
- [8] E. Jeckelmann, *Phys. Rev. B* **66**, 045114 (2002).
- [9] A. V. Rozhkov, *Eur. Phys. J. B* **47**, 193 (2005).
- [10] R. G. Pereira, J. Sirker, J.-S. Caux, R. Hagemans, J. M. Maillet, S. R. White, and I. Affleck, *J. Stat. Mech.* **2007**, P08022 (2007).